IEEE Access
Multidisciplinary | Rapid Review | Open Access Journal

Received August 30, 2021, accepted October 19, 2021, date of publication October 22, 2021, date of current version October 28, 2021.

Digital Object Identifier 10.1109/ACCESS.2021.3122234

Dual-Rate Data-Driven Virtual Reference Feedback Tuning: Improvement in Fast-Tracking Performance and Ripple-Free Design

TAKAO SATO[1], (Member, IEEE), YUTA SAKAI[1], NATSUKI KAWAGUCHI[1], AND ORLANDO ARRIETA[2]

[1]Graduate School of Engineering, University of Hyogo, Himeji, Hyogo 671-2280, Japan
[2]Research Institute of Engineering, Faculty of Engineering, University of Costa Rica, San José 11501-2060, Costa Rica

Corresponding author: Takao Sato (tsato@eng.u-hyogo.ac.jp)

This work was supported in part by the Tateisi Science and Technology Foundation, in part by Japan Society for the Promotion of Science (JSPS) KAKENHI under Grant 19K15015, and in part by the University of Costa Rica under Grant 731-B9-265.

ABSTRACT In this study, a data-driven design method is proposed for a dual-rate system, where the sampling interval of a plant output is restricted and is an integer multiple of the holding interval of a control input. In our proposed method, single-rate virtual reference feedback tuning (S-VRFT), where the holding interval is the same as the sampling interval, is extended to the dual-rate virtual reference feedback tuning (D-VRFT) system. In D-VRFT, a controller is decided using a set of input/output data used in S-VRFT, and it is easy to extend S-VRFT to D-VRFT and implement D-VRFT. In this study, intersample oscillations caused in such a dual-rate control system is prevented because a weighting filter is introduced for penalizing the control input deviation between the sampling instants. The filter is designed as an integrator for weighting the low-frequency domain. The improvement in fast-tracking performance as well as the ripple-free property are demonstrated through both the numerical and experimental results.

INDEX TERMS Data-driven design, dual-rate sampling, intersample, ripple, DC motor.

I. INTRODUCTION

In a control approach, the performance of controllers can be estimated without mathematical models or prior knowledge of the plant [1], [2]. Therefore, data-driven control methods based on the control concept have been attracted in the control engineering filed [3], [4]. In the virtual reference framework, Campi *et al.* [5] have proposed virtual reference feedback tuning (VRFT). Furthermore, owing to the usefulness of VRFT, non-minimum phase systems [6], multivariable systems [7], and the application for wastewater treatment plant control [8] have been studied.

In recent years, the networked system [9]–[11] has been applied in a wide range of areas: vehicle [12], [13], agriculture [14], construction industry [15], finance [16], healthcare [17], [18], among others. Furthermore, the data-driven approach for networked control systems has been attracted [19], [20]. In networked control systems, multiple devices are connected with networks. Most recent controllers are implemented using microcontrollers or digital signal processors, wherein the clock speed of the central processing unit used in the digital computer is very high, and the control systems can thus be operated at a high frequency. On the contrary, the intervals of the sensor data supplied through networks have insufficient speed compared to digital controllers, and the control and sampling intervals of devices are generally different [21]–[23].

In single-input-single-output (SISO) systems, when the sampling interval of a plant output is the same as the holding interval of a control input, it is referred to as a single-rate system, whereas it is referred as a dual-rate system when the intervals are different. Most of the design methods for dual-rate systems are model-based [24]–[26], and the model-based methods require a mathematical model to

The associate editor coordinating the review of this manuscript and approving it for publication was Jesus Felez.

represent the dynamic properties. Since accurate mathematical models are not always available, the control system designed based on the designs based on inaccurate models do not achieve the expected performance. In this study, a dual-rate data-driven design method is proposed for controlling SISO continuous-time systems, wherein discrete-time control input decided by a digital computer is updated at a high frequency whereas the continuous-time plant output is sampled at a low frequency. As a conventional dual-rate data-driven method, the noniterative correlation-based tuning method [27] proposed for the single-rate system has been extended to the dual-rate system [28] using the multivariable methods [29], [30]. However, in the conventional method, as the number of a set of input/output data is the same as the number of input channels, enormous control executions are required for tuning a controller when the ratio between the sampling and holding intervals is increased. In industry, the number of trial work to obtain test data should be reduced as much as possible. In contrast to the conventional dual-rate method, the proposed method, based on the VRFT approach, requires only a set of input/output data. In other words, the proposed dual-rate design method is implemented using the same data used in the conventional VRFT for the single-rate system.

In such dual-rate control systems, the plant output might oscillate between the sampling instants even when there is no steady-state error at sampling instants [31], [32]. To suppress such intersample ripples, a pre-filter is introduced herein in the proposed dual-rate method. An integrator is used for designing the pre-filter such that the difference of the control input between the sampling instants is penalized in the steady state.

The rest of this paper is organized as follows: the conventional single-rate VRFT (S-VRFT) is briefly reviewed, and the motivation of this research is provided in Section II. The design of the proposed dual-rate VRFT (D-VRFT) is realized in Section III. In Section IV, S-VRFT and D-VRFT are applied in numerical examples, respectively, and the effectiveness of D-VRFT is demonstrated. Furthermore, both S-VRFT and D-VRFT are applied to the motor control in Section V. Finally, concluding remarks are given in Section VI.

II. PROBLEM FORMULATION

A controlled plant is a SISO linear time-invariant continuous-time system, and it is controlled by a discrete-time controller. Therefore, discrete-time control input is decided using the discrete-time plant output, wherein the continuous-time plant output is sampled. In such a control system, there are two intervals: holding and sampling intervals. In the present study, the control system is designed under the following assumptions:

- The continuous-time controlled plant is a controllable and minimum phase system.
- The dynamics of the plant are unknown.

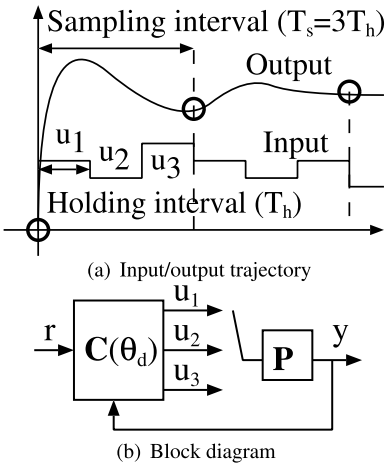

FIGURE 1. Dual-rate control system ($T_s = 3\,T_h$).

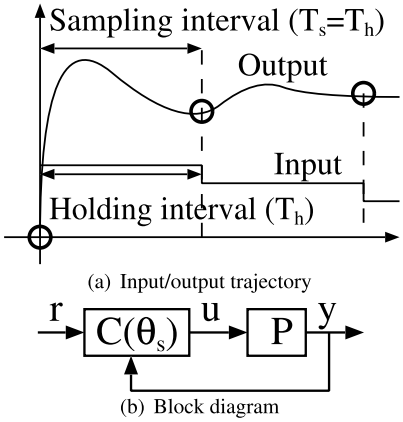

FIGURE 2. Single-rate control system ($T_s = T_h$).

- The holding interval of the control, $T_h(\in \mathbb{R}^+)$ is not limited.
- The sampling interval of the plant output, T_s is restricted, and it is assumed that $T_s = lT_h$ ($l \in \mathbb{N}^+$).
- The measurement data is not exposed to malicious attacks.

From above, the sampling interval is restricted, whereas the holding interval can be set to less than or equal to the sampling interval. Fig. 1(a) shows a schematic view of an input/output trajectory in a dual-rate system as an example of $T_s = 3T_h$. Contrary to the dual-rate system, a schematic view of an input/output trajectory in the single-rate system is shown in Fig. 2(a), where the holding interval must be increased to be equal to the sampling interval.

Herein, z^{-1} denotes the backward-shift operator, and $z^{-1}y(k) = y(k-1)$. $\otimes$ and $\odot$ denote the Kronecker and Hadamard products, respectively. $\boldsymbol{I}_n$ and $\mathbf{0}_{m,n}$ are an $n \times n$ identify matrix and an $m \times n$ zero matrix, respectively. $\mathbb{N}^+$ and $\mathbb{R}^+$ denote the spaces of positive integer and positive real numbers, respectively, and $\mathbb{R}$ denotes the space of real numbers.

A. SINGLE-RATE DESIGN

In the single-rate system, as shown in Fig. 2(a), T_h is the same as T_s, and a discrete-time SISO controlled plant model is therefore expressed as follows:

$$y(k) = P(z^{-1})u(k) \tag{1}$$

where $y(k) \in \mathbb{R}$ and $u(k) \in \mathbb{R}$ are the plant output and control signal, respectively, and $P(z^{-1})$ denotes the linear time-invariant discrete-time system.

The plant is controlled using the following control law:

$$\begin{aligned} u(k) &= C(z^{-1};\boldsymbol{\theta}_s)e(k) \\ C(z^{-1};\boldsymbol{\theta}_s) &= \boldsymbol{\beta}(z^{-1})^\top \boldsymbol{\theta}_s \\ e(k) &= r(k) - y(k) \end{aligned} \tag{2}$$

where $r(k) \in \mathbb{R}$ denotes the reference input to be followed by the discrete-time plant output. $\boldsymbol{\beta}(z^{-1})$ and $\boldsymbol{\theta}_s$ are the controller structure vector and controller parameter vector, respectively, and are provided as follows:

$$\begin{aligned} \boldsymbol{\beta}(z^{-1}) &= [\beta_1(z^{-1}) \;\; \beta_2(z^{-1}) \;\; \cdots \;\; \beta_n(z^{-1})]^\top \\ \boldsymbol{\theta}_s &= [\theta_1 \;\; \theta_2 \;\; \cdots \;\; \theta_n]^\top \end{aligned}$$

where $\beta_i(z^{-1})$ is a given transfer function ($i = 1, \cdots, n(\in \mathbb{N}^+)$), n denotes the number of elements in $\boldsymbol{\beta}(z^{-1})$, and $\theta_i \in \mathbb{R}$ is a gain. A block diagram of the single-rate control system is shown in Fig. 2(b).

The controller parameter vector is defined based on a model matching problem, and the objective function is defined as follows:

$$\begin{aligned} J_{s_{MR}}(\boldsymbol{\theta}_s) &= \left\| \left(G_s(z^{-1};\boldsymbol{\theta}_s) - M(z^{-1}) \right) W(z^{-1}) \right\|_2^2 \\ G_s(z^{-1};\boldsymbol{\theta}_s) &= \frac{P(z^{-1})C(z^{-1};\boldsymbol{\theta}_s)}{1 + P(z^{-1})C(z^{-1};\boldsymbol{\theta}_s)} \end{aligned} \tag{3}$$

where $G_s(z^{-1};\boldsymbol{\theta}_s)$ denotes the closed-loop system from the reference input to the plant output, $M(z^{-1})$ is the reference model, and $W(z^{-1})$ is a weighting function.

A common strategy between S-VRFT and D-VRFT involves optimizing the controller parameter vector of the fixed-structured controller using a set of input/output data. The optimization problem of S-VRFT is formulated as follows:

$$\begin{aligned} &\min_{\boldsymbol{\theta}_s} J_{s_{MR}}(\boldsymbol{\theta}_s) \\ &\text{s.t. given } \boldsymbol{\beta}(z^{-1}). \end{aligned} \tag{4}$$

In S-VRFT, the controller parameter vector is derived by minimizing the following objective function instead of (3):

$$\begin{aligned} J^N_{s_{VR}}(\boldsymbol{\theta}_s) &= \frac{1}{N}\sum_{k=1}^{N}(u_L(k) - C(z^{-1};\boldsymbol{\theta}_s)e_L(k))^2 \\ &= \frac{1}{N}\sum_{k=1}^{N}(u_L(k) - \boldsymbol{\varphi}_{s_L}(k)^\top \boldsymbol{\theta}_s)^2 \\ u_L(k) &= L(z^{-1})u(k) \\ \boldsymbol{\varphi}_{s_L}(k) &= \boldsymbol{\beta}(z^{-1})e_L(k) \\ e_L(k) &= L(z^{-1})\bar{e}(k) \\ \bar{e}(k) &= \bar{r}(k) - y(k) \end{aligned} \tag{5}$$

where $N \in \mathbb{N}^+$ denotes the data length. $\bar{r}(k)$ is the virtual reference such that $y(k) = M(z^{-1})\bar{r}(k)$, and $L(z^{-1})$ is a pre-filter. The minimization of (5) provides the controller parameter vector $\hat{\boldsymbol{\theta}}_{s_N}$ as follows:

$$\hat{\boldsymbol{\theta}}_{s_N} = \left[\sum_{k=1}^{N} \boldsymbol{\varphi}_{s_L}(k)\boldsymbol{\varphi}_{s_L}(k)^\top\right]^{-1} \sum_{k=1}^{N} \boldsymbol{\varphi}_{s_L}(k)u_L(k). \tag{6}$$

The controller structure is selected by the designer, and the optimal structure is generally unknown. Therefore, even though (5) which is optimized by $\hat{\boldsymbol{\theta}}_{s_N}$, differs from (3), $C(z^{-1};\hat{\boldsymbol{\theta}}_{s_N})$ is nearly optimal for (3) by a suitable selection of $L(z^{-1})$ [5].

B. MOTIVATION

In the controlled plant, as the control input can be more frequently updated than the restricted sampling interval, the tracking performance can be improved by designing VRFT in the dual-rate system. However, additional control executions to obtain dual-rate input/output data should be avoided. Therefore, D-VRFT is herein designed based on the input/output data in the single-rate system, where the holding and sampling intervals are the same. Furthermore, as intersample ripples are caused by the input deviation between the sampling instants in such a dual-rate system, a dual-rate controller is designed so that the intersample ripples are eliminated in our proposed method.

III. DUAL-RATE DESIGN

The assumption expresses that the control performance can be improved by controlling the plant with a shorter holding interval than the sampling interval as a dual-rate system. In this study, by using the lifting technique [33], the SISO dual-rate system is converted to the l-input/single-output single-rate system given as follows:

$$\begin{aligned} y(k) &= \boldsymbol{P}(z^{-1})^\top \boldsymbol{u}(k-l) \\ \boldsymbol{P}(z^{-1}) &= [P_1(z^{-1}) \;\; P_2(z^{-1}) \;\; \cdots \;\; P_l(z^{-1})]^\top \\ \boldsymbol{u}(k) &= [u_1(k) \;\; u_2(k) \;\; \cdots \;\; u_l(k)]^\top \end{aligned} \tag{7}$$

$$u_i(k) = u(k+i-1) \tag{8}$$

where $P_i(z^{-1})$ is unknown and denotes the corresponding transfer function between from $u_i(k)$ to $y(k)$ ($i = 1, \cdots, l(\in \mathbb{N}^+)$). All holding intervals of $u_i(k)$ are assumed to be same and is T_h, and the length of one step in discrete time is defined as T_h. Therefore, the control input is updated every step, whereas the plant output is sampled every l steps. Hence, $l = T_s/T_h$.

The dual-rate control law designed herein is as follows:

$$\begin{aligned} \boldsymbol{u}(k) &= \boldsymbol{C}(z^{-1};\boldsymbol{\theta}_d)e(k) \\ \boldsymbol{C}(z^{-1};\boldsymbol{\theta}_d) &= \boldsymbol{B}(z^{-1})\boldsymbol{\theta}_d \\ \boldsymbol{B}(z^{-1}) &= \boldsymbol{I}_l \otimes \boldsymbol{\beta}(z^{-1})^\top. \end{aligned} \tag{9}$$

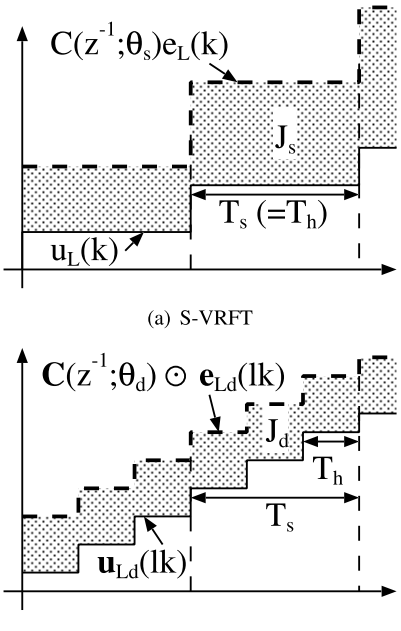

(a) S-VRFT

(b) D-VRFT ($T_s = 3T_h$)

FIGURE 3. Evaluation image of $J^N_{s_{VR}}(\theta_s)$ and $J^N_{d_{VR}}(\theta_d)$.

The above dual-rate control law is straightforwardly extended from the single-rate control law, the controller structure is set to $\boldsymbol{B}(z^{-1})$. As a result, the controller parameter vector $\boldsymbol{\theta}_d$ is the n_l-dimensional vector of parameters ($\boldsymbol{\theta}_d = [\theta_1 \ \theta_2 \ \cdots \ \theta_{n_l}]^\top$), where $n_l = n \times l$.

A block diagram of the dual-rate control system considered herein is shown in Fig. 1(b).

A. DUAL-RATE DESIGN

In D-VRFT, the controller parameter vector is decided by solving a model matching problem, where the objective function of D-VRFT is defined as follows:

$$J_{d_{MR}}(\boldsymbol{\theta}_d) = \left\| \left(G_d(z^{-1};\boldsymbol{\theta}_d) - M(z^{-1}) \right) W(z^{-1}) \right\|_2^2$$
$$G_d(z^{-1};\boldsymbol{\theta}_d) = \frac{\boldsymbol{P}(z^{-1})^\top \boldsymbol{C}(z^{-1};\boldsymbol{\theta}_d)}{1 + \boldsymbol{P}(z^{-1})^\top \boldsymbol{C}(z^{-1};\boldsymbol{\theta}_d)} \tag{10}$$

where $G_d(z^{-1};\boldsymbol{\theta}_d)$ denotes the closed-loop system in the dual-rate system. Therefore, the optimization problem of the dual-rate system is defined as follows:

$$\min_{\boldsymbol{\theta}_d} J_{d_{MR}}(\boldsymbol{\theta}_d)$$
$$\text{s.t. given } \boldsymbol{\beta}(z^{-1}). \tag{11}$$

The constrained conditions in (4) and (11) are the same as the controller of D-comprises the controller structure of S-VRFT. Even though the design objectives of S-VRFT and D-VRFT are the same, the representations of the objective functions are (3) and (10) and are different. Therefore, as shown in Fig. 3, the evaluated data in the objective functions of S-VRFT and D-VRFT are also different.

In the same manner as S-VRFT, instead of (10), the controller parameter vector is decided based on the minimization of the following function:

$$J^N_{d_{VR}}(\boldsymbol{\theta}_d) = \frac{1}{N}\sum_{k=1}^{N} \|\boldsymbol{u}_{L_d}(lk) - \boldsymbol{C}(z^{-1};\boldsymbol{\theta}_d) \odot \boldsymbol{e}_{L_d}(lk)\|_2^2$$
$$\boldsymbol{u}_{L_d}(k) = \boldsymbol{L}_d(z^{-1}) \odot \boldsymbol{u}(k)$$
$$\boldsymbol{e}_{L_d}(k) = \boldsymbol{L}_d(z^{-1})\bar{e}(k)$$
$$\boldsymbol{L}_d(z^{-1}) = [L_1(z^{-1}) \ L_2(z^{-1}) \ \cdots \ L_l(z^{-1})]^\top \tag{12}$$

where $\boldsymbol{L}_d(z^{-1})$ is the lifted vector of $L(z^{-1})$, and hence $L(z^{-1}) = \sum_{i=1}^{l} L_i(z^{-1})$. (12) is rewritten as follows:

$$J^N_{d_{VR}}(\boldsymbol{\theta}_d) = \frac{1}{N}\sum_{k=1}^{N} \|\boldsymbol{u}_{L_d}(lk) - \boldsymbol{\Phi}_{L_d}(lk)\boldsymbol{\theta}_d\|_2^2$$
$$\boldsymbol{\Phi}_{L_d}(k) = \boldsymbol{B}_{L_d}(z^{-1})e(k)$$
$$\boldsymbol{B}_{L_d}(z^{-1}) = \text{block diag}\{\boldsymbol{\beta}(z^{-1})^\top L_1(z^{-1}) \ \cdots$$
$$\cdots \ \boldsymbol{\beta}(z^{-1})^\top L_l(z^{-1})\}. \tag{13}$$

By minimizing (13), the controller parameter vector is obtained as follows:

$$\hat{\boldsymbol{\theta}}_{d_N} = \left[\sum_{k=1}^{N} \boldsymbol{\Phi}_{L_d}(lk)^\top \boldsymbol{\Phi}_{L_d}(lk)\right]^{-1} \sum_{k=1}^{N} \boldsymbol{\Phi}_{L_d}(lk)^\top \boldsymbol{u}_{L_d}(lk). \tag{14}$$

The condition of the pre-filter $L(z^{-1})$ is as the same as the S-VRFT design such that

$$|L(e^{-j\omega})|^2 = |1 - M(e^{-j\omega})|^2 |M(e^{-j\omega})|^2 |W(e^{-j\omega})|^2 \frac{1}{\Phi_u}, \quad \forall\omega \in [-\pi;\pi] \tag{15}$$

where Φ_u is the spectral density of $u(k)$.

B. RIPPLE-FREE DUAL-RATE DESIGN

In D-VRFT, as the control input can be changed between the sampling instants, the intersample output might oscillate. To resolve the intersample ripple problem, the deviation of the control input between the sampling instants as well as the control error are evaluated. In this study, by introducing $J_{u_{MR}}(\boldsymbol{\theta}_d)$, wherein input deviation $(u_i(k) - u_{i+1}(k))$ is penalized, the objective function of the dual-rate design is extended as follows:

$$J_{r_{MR}}(\boldsymbol{\theta}_d) = J_{d_{MR}}(\boldsymbol{\theta}_d) + J_{u_{MR}}(\boldsymbol{\theta}_d) \tag{16}$$
$$J_{u_{MR}}(\boldsymbol{\theta}_d) = \left\| \bar{\boldsymbol{C}}(z^{-1};\boldsymbol{\theta}_d) P(z^{-1}) W_u(z^{-1}) \right\|_2^2 \tag{17}$$
$$P(z^{-1}) = \sum_{i=1}^{l} P_i(z^{-1})$$
$$\bar{\boldsymbol{C}}(z^{-1};\boldsymbol{\theta}_d) = \boldsymbol{D}_l \boldsymbol{C}(z^{-1};\boldsymbol{\theta}_d)$$
$$= [\bar{C}_1(z^{-1};\boldsymbol{\theta}_d) \ \cdots \ \bar{C}_{l-1}(z^{-1};\boldsymbol{\theta}_d)]^\top$$
$$\bar{C}_i(z^{-1};\boldsymbol{\theta}_d) = C_i(z^{-1};\boldsymbol{\theta}_d) - C_{i+1}(z^{-1};\boldsymbol{\theta}_d)$$
$$\boldsymbol{D}_l = [\boldsymbol{I}_{l-1} \ \boldsymbol{0}_{l-1,1}] - [\boldsymbol{0}_{l-1,1} \ \boldsymbol{I}_{l-1}] \tag{18}$$

where $W_u(z^{-1})$ is a weighting function. In D-VRFT, as the controller parameter vector is optimized to have the sampled output follow the reference model output, the control input vector is generated by evaluating $\boldsymbol{C}(z^{-1};\boldsymbol{\theta}_d)(M(z^{-1})r(k) - y(k))$. Therefore, as the design of $J_{u_{MR}}(\boldsymbol{\theta}_d)$, the evaluation of $\bar{\boldsymbol{C}}(z^{-1};\boldsymbol{\theta}_d)(M(z^{-1})r(k) - y(k))$ might be suitable. However, evaluating $\bar{\boldsymbol{C}}(z^{-1};\boldsymbol{\theta}_d)y(k)$ is enough. This is because the suppression of control input deviation should be prevented in the transient state for high-tracking performance, and $M(z^{-1})$ is designed so that the plant output converges to the reference input in the steady state. Therefore, the evaluation of $\bar{\boldsymbol{C}}(z^{-1};\boldsymbol{\theta}_d)M(z^{-1})r(k)$ is useless in $J_{u_{MR}}(\boldsymbol{\theta}_d)$.

As a result, the ripple-free dual-rate controller is designed by solving the following optimization problem:

$$\begin{aligned} &\min_{\boldsymbol{\theta}_d} J_{r_{MR}}(\boldsymbol{\theta}_d) \\ &\text{s.t. given } \boldsymbol{\beta}(z^{-1}). \end{aligned} \tag{19}$$

As the plant model is included in the objective function (16), the problem cannot be directly solved. Therefore, the controller parameter vector is obtained based on the minimization of the following function:

$$J^N_{r_{VR}}(\boldsymbol{\theta}_d) = J^N_{d_{VR}}(\boldsymbol{\theta}_d) + J^N_{u_{VR}}(\boldsymbol{\theta}_d) \tag{20}$$

$$\begin{aligned} J^N_{u_{VR}}(\boldsymbol{\theta}_d) &= \frac{1}{N}\sum_{k=1}^{N} \|\bar{\boldsymbol{C}}(z^{-1};\boldsymbol{\theta}_d)y_{L_u}(k)\|_2^2 \\ y_{L_u}(k) &= L_u(z^{-1})y(k) \end{aligned} \tag{21}$$

where $L_u(z^{-1})$ is a pre-filter. From the composition of $\boldsymbol{C}(z^{-1};\boldsymbol{\theta}_d)$, (20) is rewritten as follows:

$$\begin{aligned} J^N_{r_{VR}}(\boldsymbol{\theta}_d) &= \frac{1}{N}\sum_{k=1}^{N} \|\boldsymbol{u}_{L_d}(lk) - \boldsymbol{\Phi}_{L_d}(lk)\boldsymbol{\theta}_d\|_2^2 \\ &\quad + \|\bar{\boldsymbol{\Phi}}_{L_u}(lk)\boldsymbol{\theta}_d\|_2^2 \\ \bar{\boldsymbol{\Phi}}_{L_u}(k) &= \bar{\boldsymbol{B}}(z^{-1})y_{L_u}(k) \\ \bar{\boldsymbol{B}}(z^{-1}) &= \left[\boldsymbol{I}_{l-1}\otimes\boldsymbol{\beta}(z^{-1})\ \boldsymbol{0}_{l-1,n}\right] \\ &\quad - \left[\boldsymbol{0}_{l-1,n}\quad \boldsymbol{I}_{l-1}\otimes\boldsymbol{\beta}(z^{-1})\right]. \end{aligned} \tag{22}$$

The minimization of (22) provides the controller parameter vector as follows:

$$\begin{aligned} \hat{\boldsymbol{\theta}}_{d_N} = &\left[\sum_{k=1}^{N}\boldsymbol{\Phi}_{L_d}(lk)^\top\boldsymbol{\Phi}_{L_d}(lk) + \sum_{k=1}^{N}\bar{\boldsymbol{\Phi}}_{L_u}(lk)^\top\bar{\boldsymbol{\Phi}}_{L_u}(lk)\right]^{-1} \\ &\times\sum_{k=1}^{N}\boldsymbol{\Phi}_{L_d}(lk)^\top\boldsymbol{u}_{L_d}(lk). \end{aligned} \tag{23}$$

Filter $L_u(z^{-1})$ is decided based on the relation between $J_{u_{MR}}(\boldsymbol{\theta}_d)$ and $J^N_{u_{VR}}(\boldsymbol{\theta}_d)$. $J_{u_{MR}}(\boldsymbol{\theta}_d)$ is rewritten as follows:

$$\begin{aligned} J_{u_{MR}}(\boldsymbol{\theta}_d) = \frac{1}{2\pi}\int_{-\pi}^{\pi}\sum_{i=1}^{l-1}&|\bar{C}_i(e^{-j\omega};\boldsymbol{\theta}_d)|^2|P(e^{-j\omega})|^2 \\ &\times|W_u(e^{-j\omega})|^2\,d\omega \end{aligned}$$

where the function is simplified by omitting $e^{-j\omega}$:

$$J_{u_{MR}}(\boldsymbol{\theta}_d) = \frac{1}{2\pi}\int_{-\pi}^{\pi}\sum_{i=1}^{l-1}|\bar{C}_i(\boldsymbol{\theta}_d)|^2|P|^2|W_u|^2 d\omega. \tag{24}$$

In contrast to $J_{u_{MR}}(\boldsymbol{\theta}_d)$, when $N\to\infty$, $J^N_{u_{VR}}(\boldsymbol{\theta}_d)$ is rewritten as follows:

$$\lim_{N\to\infty} J^N_{u_{VR}}(\boldsymbol{\theta}_d) = J_{u_{VR}}(\boldsymbol{\theta}_d) = E[\|\bar{\boldsymbol{C}}(z^{-1};\boldsymbol{\theta}_d)y_{L_u}(k)\|_2^2]. \tag{25}$$

Furthermore,

$$J_{u_{VR}}(\boldsymbol{\theta}_d) = \frac{1}{2\pi}\int_{-\pi}^{\pi}\sum_{i=1}^{l-1}|\bar{C}_i(\boldsymbol{\theta}_d)|^2|L_u|^2|P|^2\Phi_u d\omega.$$

The comparison of (24) with (26) provides the condition to be satisfied by $L_u(z^{-1})$ as follows:

$$|L_u|^2 = |W_u|^2\frac{1}{\Phi_u},\quad \forall\omega\in[-\pi,\pi]. \tag{26}$$

where $W_u(z^{-1})$ is designed as an integrator to suppress the input deviation in the steady state.

In D-VRFT, when l is 1, the designed controller of D-VRFT is the same as that of S-VRFT. Therefore, D-VRFT is a generalized method, including S-VRFT. When S-VRFT is designed using D-VRFT, $J^N_{u_{VR}}$ is not evaluated, and $J^N_{r_{VR}} = J^N_{d_{VR}}$.

IV. SIMULATION EXAMPLE

Using a set of input/output data, D-VRFT (the proposed dual-rate VRFT) and S-VRFT (the conventional single-rate VRFT) are designed, and the control performance are compared.

Consider a plant model given as follows:

$$P(s) = \frac{\omega_n^4}{(s^2+2\zeta\omega_n s+\omega_n^2)^2} \tag{27}$$

where ζ and ω_n are 0.3 and 5, respectively. In the design of S-VRFT and D-VRFT, the tracking performance is evaluated by using the following reference model:

$$M(s) = \frac{1}{0.3s+1}.$$

The gain characteristics of the controlled plant and the reference models are shown in Fig. 4, wherein the dashed and solid lines denote the reference model and plant model characteristics, respectively.

The sampling interval of the plant output, T_s, is assumed to be restricted 0.5 seconds, whereas the holding interval of the control input, T_h, is not limited. In both S-VRFT and D-VRFT, the controller is designed using the same single-rate data, where $T_h = T_s$, and a random binary input signal of length $N = 512$ is fed to the open-loop plant. Based on the collected input/output data, the controller parameter vector is decided for the reference model. To design the PID control law, the controller structure is

$$\boldsymbol{\beta}(z^{-1}) = [1\ \ T_s/(1-z^{-l})\ \ (1-z^{-l})/T_s]^\top, \tag{28}$$

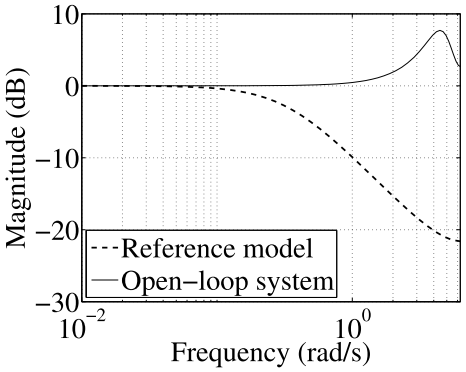

(a) Slow reference model

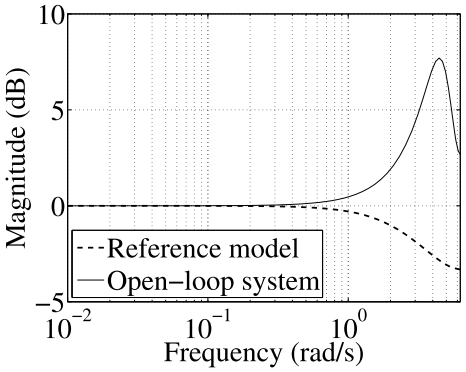

(b) Fast reference model

FIGURE 4. Gain characteristics of the controlled plant and the reference models.

TABLE 1. Obtained $\hat{\theta}_{d_N}$ ($\times 10^{-3}$).

$l=1$ (S-VRFT)					
θ_1	85.1	θ_2	138	θ_3	−14.9
$l=2$ (D-VRFT, $W_u(z^{-1})=0$)					
θ_1	−249	θ_2	1470	θ_3	63.2
θ_4	−274	θ_5	387	θ_6	2.44
$l=2$ (D-VRFT, $W_u(z^{-1})=\frac{1}{1-z^{-1}}$)					
θ_1	−98.2	θ_2	551	θ_3	13.5
θ_4	−98.2	θ_5	551	θ_6	13.2
$l=5$ ($W_u(z^{-1})=\frac{1}{1-z^{-1}}$)					
θ_1	−129	θ_2	624	θ_3	18.2
θ_4	−129	θ_5	624	θ_6	18.1
θ_7	−129	θ_8	624	θ_9	17.9
θ_{10}	−129	θ_{11}	624	θ_{12}	17.8
θ_{13}	−129	θ_{14}	624	θ_{15}	17.7

indicating $n=3$. The reference input is 1, and $W(z^{-1})$ is set to 1.

The obtained controller parameters are shown in Table 1, where l is set to 1, 2, and 5; furthermore, the controller of $l=2$ with $W_u(z^{-1})=0$ is designed to confirm the ripple-free effect. In Table 1, θ_{1+i}, θ_{2+i} and θ_{3+i} are the proportional, integral and derivative gains, respectively, where $i=3(j-1)$, and $j\in\{1,\cdots,l\}$. In the designs of D-VRFT except for $W(z^{-1})=0$, the proportional gains are the same, the integral gains are also the same, and the derivative gains

TABLE 2. Control performance index values ($\times 10^{-2}$).

l	J_d
1 (S-VRFT)	37.7
2 (D-VRFT, $W_u(z^{-1})=0$)	3.51
2 (D-VRFT, $W_u(z^{-1})=\frac{1}{1-z^{-1}}$)	7.99
5 (D-VRFT, $W_u(z^{-1})=\frac{1}{1-z^{-1}}$)	6.57

are almost the same. On the other hand, the controller parameters with $l=2$ and $W(z^{-1})=0$ are considerably different.

Fig. 5 and Fig. 6 show the output and input responses, respectively, and the magnitude Bode plots are shown in Fig. 7. Comparing Fig. 7(a) with Fig. 7(b), Fig. 7(c) and Fig. 7(d), the difference between the reference model with the closed-loop system is the worst for Fig. 7(a). In Fig. 5, the dashed lines denote the discrete-time response of the reference model output and the solid line and the circle denote the intersample output and the sampled output, respectively. Fig. 5(a) shows that S-VRFT (D-VRFT with $l=1$) is insufficient for fast tracking, although there is no ripple since the control input does not oscillate as shown in Fig. 6(a). Fig. 5(b) shows that the intersample output oscillates at 2Hz since the control input oscillates as shown in Fig. 6(b), although the response of the sampled output is quick. From Fig. 5(c) and Fig. 5(d), there is no intersample ripple as the input deviation is evaluated, and Fig. 6(c) and Fig. 6(d) show that the control input does not oscillate. Furthermore, the output response is improved with large l by the comparison of Fig. 5(c) with Fig. 5(d).

For a quantitative evaluation, the performance index is defined as follows:

$$J_d=\frac{1}{N_{data}}\sum_{k=1}^{N_{data}}|M(z^{-1})r(lk)-y(lk)| \tag{29}$$

where N_{data} denotes the number of the sampling step 30 in the simulation. The evaluated values are summarized in Table 2. The table shows that the difference of the tracking performance is large. Furthermore, the index values of the ripple-free design in $1\le l\le 50$ are plotted in Fig. 8. The figure shows that the larger l is, the better the performance is.

V. EXPERIMENT

S-VRFT and D-VRFT are applied to a motor control system shown in Fig. 9. The components of the system are summarized in Table 3(a). The rotation velocity of the cylinder is measured by the sensor included in Motor 1, and is sent to the controller, the current to be supplied to Motor1 is decided by the controller using the measured data, and Motor1 is actuated by the calculated current supplied by the motor driver. In the system, Motor2 is not actuated and is just load although the cylinder can be rotated by Motor2 as well as Motor1 since Motor2 is connected to the shaft through the belt.

In the present study, D-VRFT with $W_u(z^{-1})=\frac{1}{1-z^{-1}}$ is compared with both S-VRFT and D-VRFT with $W_u(z^{-1})=0$ in V-A and V-B, respectively.

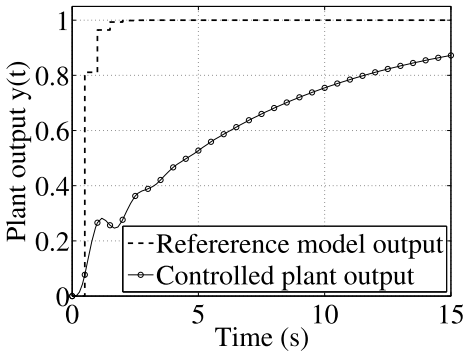

(a) $l = 1$ (S-VRFT)

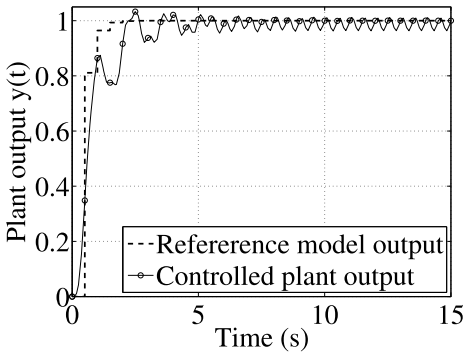

(b) $l = 2$ (D-VRFT, $W_u(z^{-1}) = 0$)

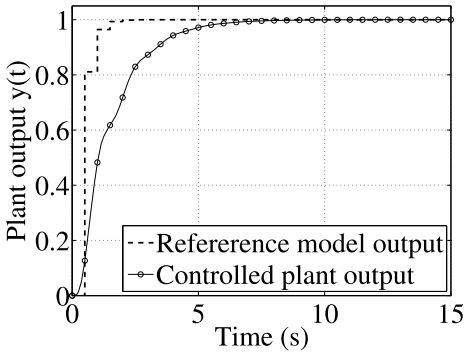

(c) $l = 2$ (D-VRFT, $W_u(z^{-1}) = \frac{1}{1-z^{-1}}$)

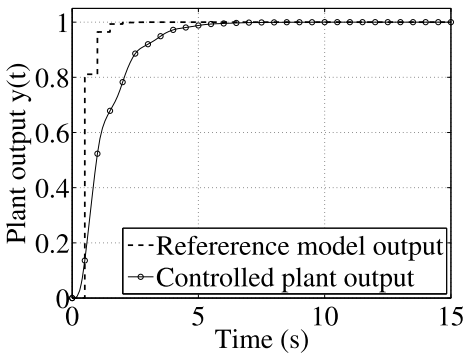

(d) $l = 5$ (D-VRFT, $W_u(z^{-1}) = \frac{1}{1-z^{-1}}$)

FIGURE 5. Output responses for the fast reference model.

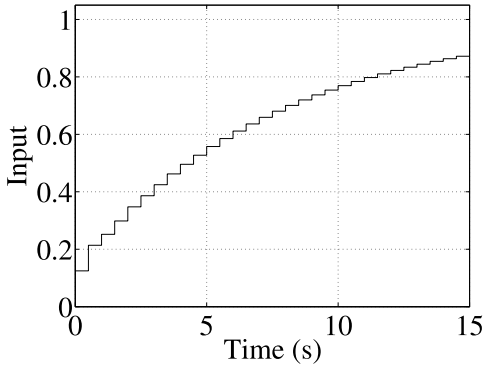

(a) $l = 1$ (S-VRFT)

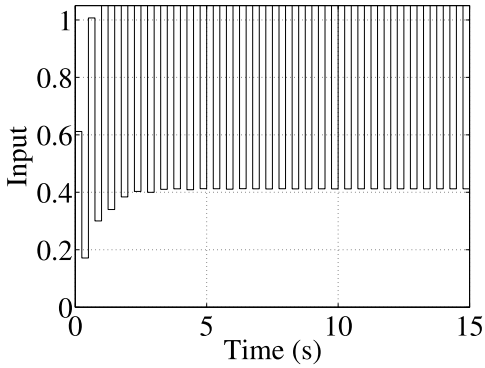

(b) $l = 2$ (D-VRFT, $W_u(z^{-1}) = 0$)

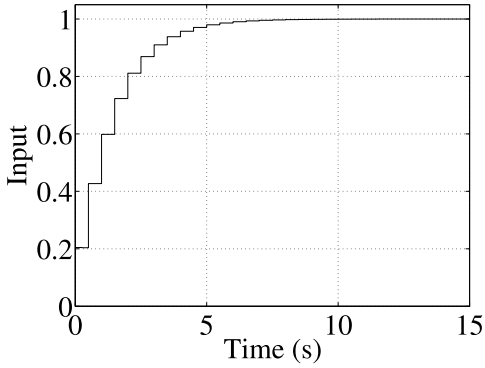

(c) $l = 2$ (D-VRFT, $W_u(z^{-1}) = \frac{1}{1-z^{-1}}$)

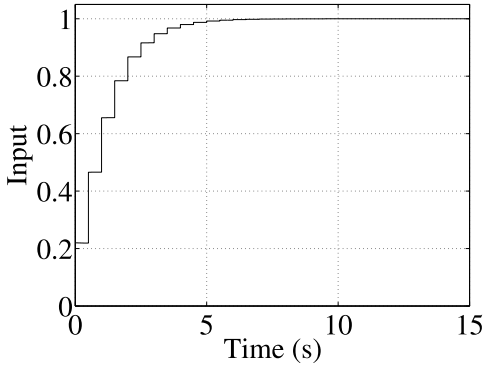

(d) $l = 5$ (D-VRFT, $W_u(z^{-1}) = \frac{1}{1-z^{-1}}$)

FIGURE 6. Input responses for the fast reference model.

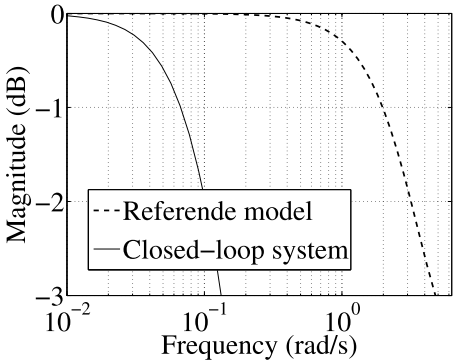

(a) $l = 1$ (S-VRFT)

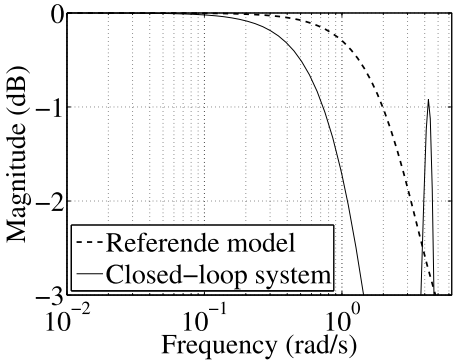

(b) $l = 2$ (D-VRFT, $W_u(z^{-1}) = 0$)

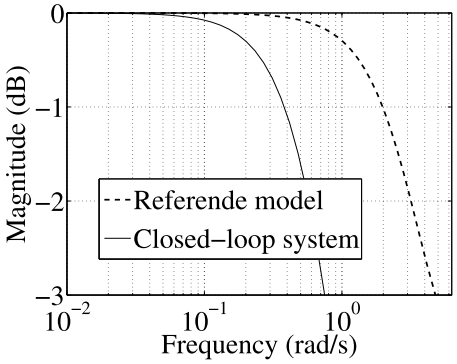

(c) $l = 2$ (D-VRFT, $W_u(z^{-1}) = \frac{1}{1-z^{-1}}$)

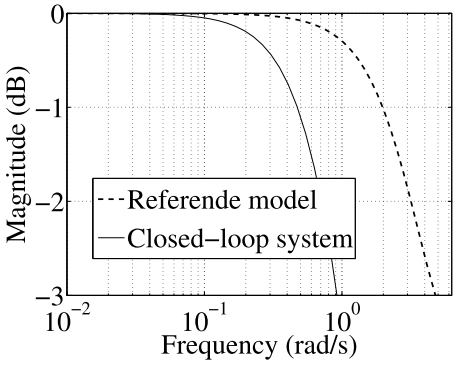

(d) $l = 5$ (D-VRFT, $W_u(z^{-1}) = \frac{1}{1-z^{-1}}$)

FIGURE 7. Gain characteristics for the fast reference model.

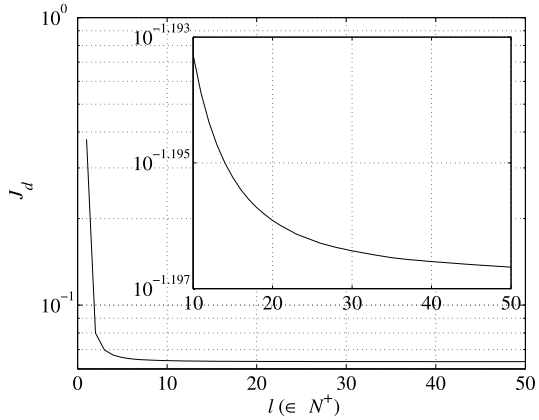

FIGURE 8. Index value J_d using D-VRFT.

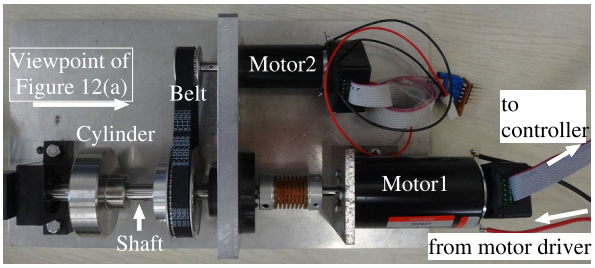

FIGURE 9. Motor control system.

TABLE 3. Component elements of the laboratory equipment.

(a) Original system

Motor1	Maxon, DC motor(200627)
Motor2	Maxon, DC motor(135043)
Belt	Misumi, Power Grip GT Belt, 3GT Type, 252-3GT-9
Cylinder	Austenitic stainless steel (diameter:50mm, width:15mm)
Motor driver	Maxon, ESCON 50/5 (current control mode)
Power source	ALINCO, DM-320W
Controller	Cypress, PSoC 5LP

(b) Additional pulley

Pulley	Misumi, Backside Tension Idler Pulley Center Bearing (AFBD11.5-25)

A. RIPPLE SUPPRESSION BY CONTROLLER DESIGN

The PI control law is designed from input/output data so that the rotation velocity of the cylinder is kept to be a specified value. In the pre-experiment to obtain the input/output data for tuning the controller parameter, the rotation system is actuated using the random input signal shown in Fig. 10(b), and the measured rotation velocity is shown in Fig. 10(a). The reference model is given as follows:

$$M(s) = \frac{\omega_n^2}{s^2 + 2\zeta\omega_n s + \omega_n^2}, \tag{30}$$

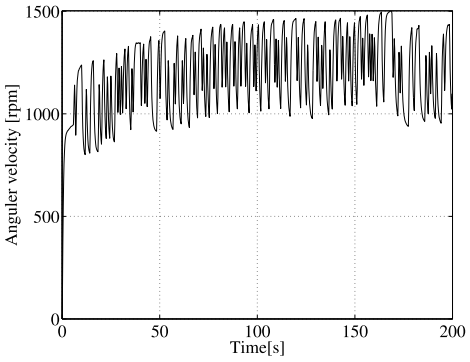

(a) Rotation velocity

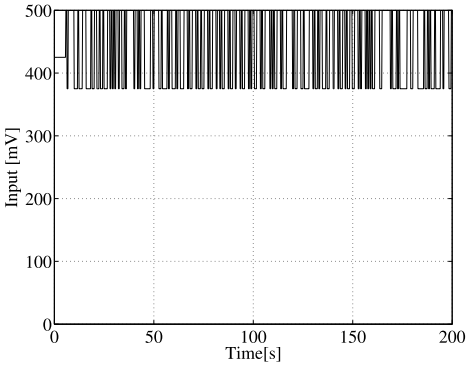

(b) Input voltage

FIGURE 10. Pre-experiment.

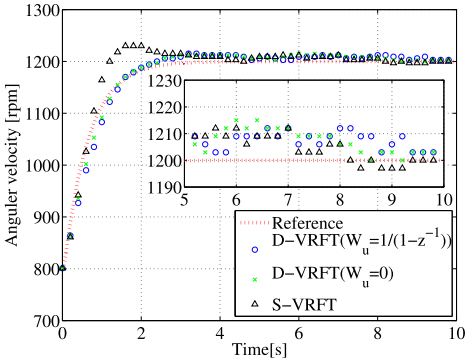

(a) Rotation velocity (discrete-time sampled data)

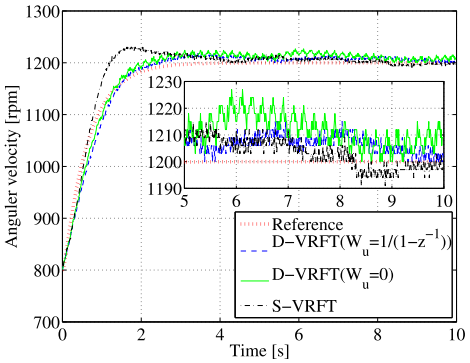

(b) Rotation velocity (continuous-time data)

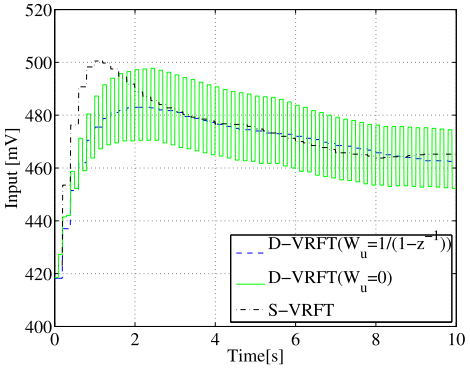

(c) Input voltage

FIGURE 11. Experimental result.

where ζ and ω_n are 2 and 6, respectively, and the controller structure is given as follows:

$$\boldsymbol{\beta}(z^{-1}) = [1 \;\; T_s/(1-z^{-l})]^\top. \tag{31}$$

To control in the linear domain, the controller parameters are decided using the input/output data after 10 seconds as the initial state. In the system, because the sensor is a rotary encoder, the sampling interval of the measured rotation velocity could not be set less than 0.2 seconds to measure the velocity accurately. On the other hand, the holding interval of the input signal can be less than the sampling interval. Therefore, the holding interval is 0.1 seconds when D-VRFT is used, whereas the holding interval is 0.2 seconds when S-VRFT is used.

The conventional dual-rate data-driven method [28] is not designed using one set of data shown in Fig. 10 since two sets of control data are required. On the other hand, the proposed dual-rate method (D-VRFT) is designed using one set of control data.

The obtained controller parameters are shown in Table 4. In design of D-VRFT, when $W_u(z^{-1}) = 0$, $\theta_1 \neq \theta_3$, and $\theta_2 \neq \theta_4$. On the other hand, when $W_u(z^{-1})$ is designed as an integrator, $\theta_1 = \theta_3$, and $\theta_2 = \theta_4$.

The control results using the tuning parameters are shown in Fig. 11(a), Fig. 11(b) and Fig. 11(c), where the rotation velocity is controlled to be 1200[rpm] from 800[rpm] as the initial state. As shown in Fig. 11(a), the trajectory of the rotation velocity using D-VRFT follows that of the reference model output at sampling instants, and the tracking performance using S-VRFT is degraded compared with D-VRFT. However, since the input signal using D-VRFT

TABLE 4. Obtained $\hat{\theta}_{d_N}$ in experiment.

$l = 1$ (S-VRFT)			
θ_1	-0.162	θ_2	0.335
$l = 2$ (D-VRFT, $W_u(z^{-1}) = 0$)			
θ_1	-0.165	θ_2	0.269
θ_3	0.0311	θ_4	0.253
$l = 2$ (D-VRFT, $W_u(z^{-1}) = \frac{1}{1-z^{-1}}$)			
θ_1	-0.0685	θ_2	0.261
θ_3	-0.0685	θ_4	0.261

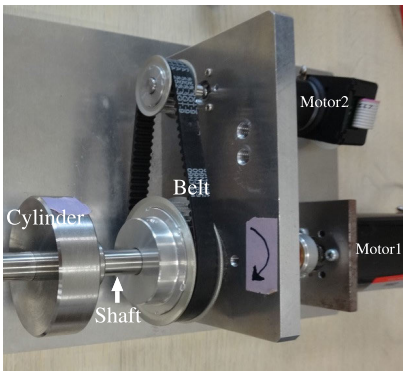

(a) System before modification

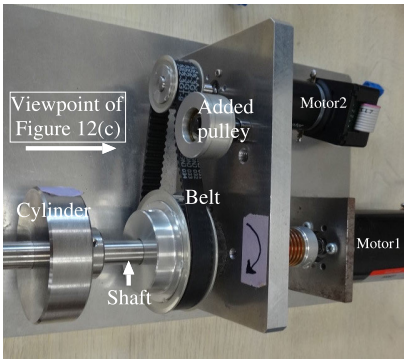

(b) Modified system

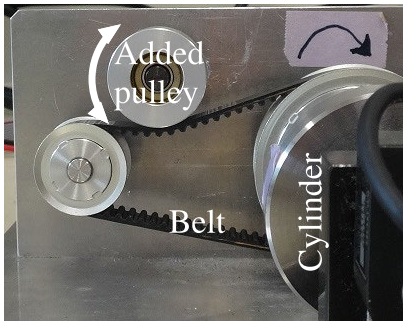

(c) Added pulley

FIGURE 12. Hardware modification.

with $W_u(z^{-1}) = 0$ oscillates as shown in Fig. 11(c), the intersample response oscillates as shown in Fig. 11(b) even though the sampled output follows the reference model output. On the other hand, $W_u(z^{-1})$ is designed an integrator, the intersample output follows to the reference model output without oscillation since the input signal does not oscillate between the sampling instants.

The experimental results are quantitatively evaluated using (29), where N_{data} is 1000. The index values are summarized in Table 4. From the table, in the discrete-time domain, D-VRFT is superior than S-VRFT, and D-VRFT with $W_u(z^{-1}) = 0$ is the best. Using D-VRFT with $W_u(z^{-1}) = \frac{1}{1-z^{-1}}$, the intersample response as well as the sampled response are well controlled, although the index value is slightly degraded compared with D-VRFT with $W_u(z^{-1}) = 0$.

TABLE 5. Index values of the experiment.

l	J_d
1 (S-VRFT)	39.3
2 (D-VRFT, $W_u(z^{-1}) = 0$)	34.7
2 (D-VRFT, $W_u(z^{-1}) = \frac{1}{1-z^{-1}}$)	35.1

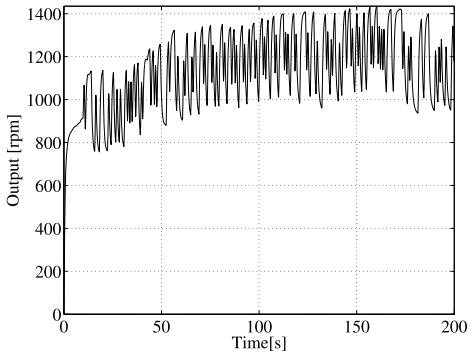

(a) Rotation velocity

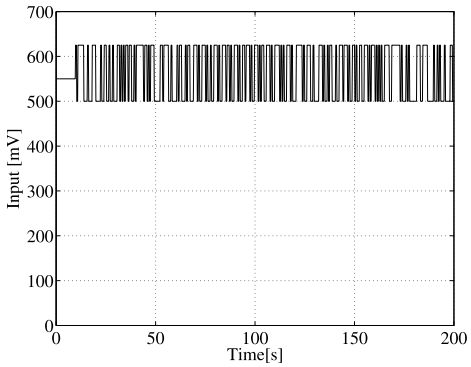

(b) Input voltage

FIGURE 13. Pre-experiment using an additional pulley.

B. RIPPLE SUPPRESSION BY HARDWARE MODIFICATION

In V-A, the intersample ripple occurred using D-VRFT with $W_u(z^{-1}) = 0$ is resolved by penalizing the control input deviation, and a software-based solution is given. Contrary to V-A, the experimental setup is modified to suppress the intersample ripple.

By adding a pulley detailed in Table 3(b) to the original system shown as Fig. 12(a), a modified system as shown in Fig. 12(b) is obtained. In the modified system, the tension of the belt is increased because of the added pulley as shown in Fig. 12(c).

On the same controller design conditions as V-A, the input/output data for tuning the controller parameter are obtained as shown in Fig. 13. The tuned controller parameters based on the input/output data and (30) with $\zeta = 2$ and $\omega_n = 3$ are summarized in Table 6.

The controlled results of the modified system are shown in Fig. 14. The output trajectories obtained using D-VRFT, where $W_u(z^{-1})$ is 0 and an integrator, respectively, follow the reference trajectory better than S-VRFT. Furthermore, as shown in Fig. 14(b), there is no intersample ripple using

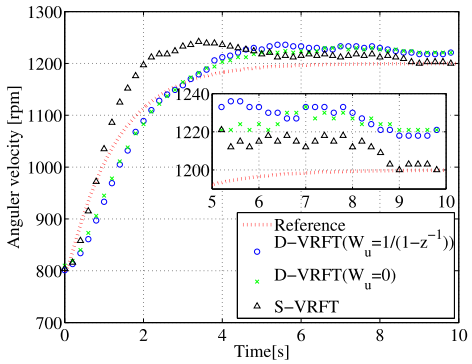

(a) Rotation velocity (discrete-time sampled data)

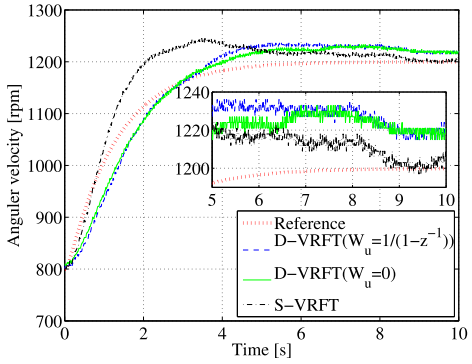

(b) Rotation velocity (continuous-time data)

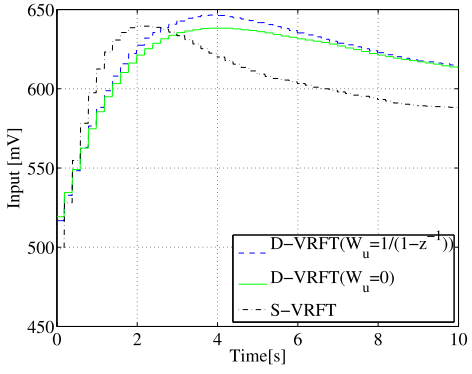

(c) Input voltage

FIGURE 14. Experimental result using an additional pulley.

TABLE 6. Obtained $\hat{\theta}_{d_N}$ in experiment using an added pulley.

$l = 1$ (S-VRFT)			
θ_1	-0.176	θ_2	0.291
$l = 2$ (D-VRFT, $W_u(z^{-1}) = 0$)			
θ_1	-0.129	θ_2	0.161
θ_3	-0.0188	θ_4	0.154
$l = 2$ (D-VRFT, $W_u(z^{-1}) = \frac{1}{1-z^{-1}}$)			
θ_1	-0.0778	θ_2	0.158
θ_3	-0.0778	θ_4	0.158

D-VRFT with $W_u(z^{-1}) = 0$. This is because θ_1 is close to θ_3 and θ_2 is also close to θ_4 as shown in Table 6. Fig. 14(c) shows that the control input is larger than Fig. 11(c), even though the target rotation velocity is the same because the rotation load is increased by the added pulley. The evaluated values using (29) are summarized in Table 7. The table shows that D-VRFT is superior than S-VRFT.

TABLE 7. Index values of the experiment using an additional pulley.

l	J_d
1 (S-VRFT)	57.0
2 (D-VRFT, $W_u(z^{-1}) = 0$)	46.1
2 (D-VRFT, $W_u(z^{-1}) = \frac{1}{1-z^{-1}}$)	50.4

VI. CONCLUSION

In this study, we proposed a data-driven design method for a SISO time-invariant dual-rate system, wherein the sampling interval is restricted whereas the holding interval is not limited. For such a system, D-VRFT is proposed, where the control input is more frequently updated than the restricted sampling interval. The proposed method has three main features: D-VRFT is

- designed using the same single-rate input/output data used in S-VRFT,
- and is a ripple-free method.

The features are confirmed through numerical as well as experimental examples by designing S-VRFT and D-VRFT, respectively.

Since the computation of the inverse matrix in the proposed method depends on the initial input and output data, the optimization method using regularization is an issue to be considered in the future. In addition, the development of optimization-based control is also an issue for the future.

In this study, all hold intervals between the sampling instants are set to equivalent, whereas non-uniform intervals can be accepted as the multi-rate system. Our future work involves extending our proposed method to non-uniform interval systems.

The performance using the proposed model-free method designed directly from the data can be better than model-based approaches using incorrect model. In reinforcement learning such as Q-learning, a model-free design may improve performance rather than a model-fixed design. Therefore, in the future, it is expected that model-free methods will be developed in the field of reinforcement learning.

REFERENCES

[1] M. G. Safonov and T.-C. Tsao, "The unfalsified control concept and learning," *IEEE Trans. Autom. Control*, vol. 42, no. 6, pp. 843–847, Jun. 1997.
[2] M. Jun and M. G. Safonov, "Automatic PID tuning: An application of unfalsified control," in *Proc. IEEE Int. Symp. Comput. Aided Control Syst. Design*, Aug. 1999, pp. 328–333.
[3] Z.-S. Hou and Z. Wang, "From model-based control to data-driven control: Survey, classification and perspective," *Inf. Sci.*, vol. 235, pp. 3–35, Jun. 2013.
[4] S. Formentin, K. van Heusden, and A. Karimi, "A comparison of model-based and data-driven controller tuning," *Int. J. Adapt. Control Signal Process.*, vol. 28, no. 10, pp. 882–897, 2012.
[5] M. Campi, A. Lecchini, and S. Savaresi, "Virtual reference feedback tuning (VRFT): A direct method for the design of feedback controllers," *Automatica*, vol. 38, pp. 1337–1346, 2002.

[6] L. Campestrini, D. Eckhard, M. Gevers, and A. S. Bazanella, "Virtual reference feedback tuning for non-minimum phase plants," *Automatica*, vol. 47, no. 8, pp. 1778–1784, 2011.
[7] G. R. Goncalves da Silva, L. Campestrini, and A. S. Bazanella, "Multivariable VRFT: An approach for systems with non-minimum phase transmission zeros," in *Proc. IEEE Conf. Control Appl. (CCA)*, Sep. 2016, pp. 1324–1329.
[8] J. D. Rojas, X. Flores-Alsina, U. Jeppsson, and R. Vilanova, "Application of multivariate virtual reference feedback tuning for wastewater treatment plant control," *Control Eng. Pract.*, vol. 20, no. 5, pp. 499–510, May 2012.
[9] W. Chen and L. Qiu, "Stabilization of multirate networked control systems," in *Proc. IEEE Conf. Decis. Control Eur. Control Conf.*, Dec. 2011, pp. 5274–5280.
[10] H. Katayama, "Design of consensus controllers for multi-rate sampled-data strict-feedback multi-agent systems," *IFAC-PapersOnLine*, vol. 48, pp. 157–162, Dec. 2015.
[11] C.-J. Li, X.-R. Yang, and J. Zhao, "Multi-rate design of networked predictive controller and its application for consensus of networked multi-agent systems with delays," in *Proc. Chin. Control Conf. (CCC)*, Jul. 2019, pp. 5474–5479.
[12] J. Bach, J. Langner, S. Otten, M. Holzapfel, and E. Sax, "Data-driven development, a complementing approach for automotive systems engineering," in *Proc. IEEE Int. Syst. Eng. Symp. (ISSE)*, Oct. 2017, pp. 1–6.
[13] K. Zhang, R. Su, H. Zhang, and Y. Tian, "Adaptive resilient event-triggered control design of autonomous vehicles with an iterative single critic learning framework," *IEEE Trans. Neural Netw. Learn. Syst.*, early access, Feb. 3, 2021, doi: 10.1109/TNNLS.2021.3053269.
[14] M. N. I. Sarker, M. Wu, B. Chanthamith, S. Yusufzada, D. Li, and J. Zhang, "Big data driven smart agriculture: Pathway for sustainable development," in *Proc. 2nd Int. Conf. Artif. Intell. Big Data (ICAIBD)*, May 2019, pp. 60–65.
[15] F. R. Correa, "Cyber-physical systems for construction industry," in *Proc. IEEE Ind. Cyber-Phys. Syst. (ICPS)*, May 2018, pp. 392–397.
[16] S. Kurt, J. Heitz, N. Bundi, and W. Breymann, "Large-scale data-driven financial risk modeling using big data technology," in *Proc. IEEE/ACM 5th Int. Conf. Big Data Comput. Appl. Technol. (BDCAT)*, Dec. 2018, pp. 206–207.
[17] D. Gotz and D. Borland, "Data-driven healthcare: Challenges and opportunities for interactive visualization," *IEEE Comput. Graph. Appl.*, vol. 36, no. 3, pp. 90–96, May 2016.
[18] Q. Cai, H. Wang, Z. Li, and X. Liu, "A survey on multimodal data-driven smart healthcare systems: Approaches and applications," *IEEE Access*, vol. 7, pp. 133583–133599, 2019.
[19] Y. Xia, W. Xie, B. Liu, and X. Wang, "Data-driven predictive control for networked control systems," *Inf. Sci.*, vol. 235, pp. 45–54, Jun. 2013.
[20] S. Zhen, Z. Hou, and C. Yin, "A novel data-driven predictive control for networked control systems with random packet dropouts," in *Proc. 6th Data Driven Control Learn. Syst. (DDCLS)*, May 2017, pp. 335–340.
[21] X. Zhao, W. Zhang, H. Zhang, and Q. Chen, "Modeling of multirate input and output networked control system," in *Proc. WRI Global Congr. Intell. Syst.*, 2009, pp. 258–263.
[22] H. Beikzadeh and H. J. Marquez, "Multirate output feedback control of nonlinear networked control systems," *IEEE Trans. Autom. Control*, vol. 60, no. 7, pp. 1939–1944, Jul. 2015.
[23] H. Beikzadeh and H. J. Marquez, "Robust sampled-data bilateral teleoperation: Single-rate and multirate stabilization," *IEEE Trans. Control Netw. Syst.*, vol. 5, no. 1, pp. 675–687, Mar. 2018.
[24] E. A. Escolastico, M. Guinaldo, A. Cuenca, J. Salt, and S. Dormido, "Anytime optimal control strategy for multi-rate systems," *IEEE Access*, vol. 5, pp. 2790–2797, 2017.
[25] T. Furusaka, T. Sato, N. Kawaguchi, N. Araki, and Y. Konishi, "Consensus control of dual-rate multi-agent systems with quantized communication," *IEEE Access*, vol. 8, pp. 97557–97563, 2020.
[26] X. Chi, Y. Zhang, and X. Jia, "Event-triggered predictive control for networked systems based on a dual-rate sampling switched observer," *IEEE Access*, vol. 9, pp. 89580–89592, 2021.
[27] A. Karimi, K. van Heusden, and D. Bonvin, "Non-iterative data-driven controller tuning using the correlation approach," in *Proc. Eur. Control Conf. (ECC)*, Jul. 2007, pp. 5189–5195.
[28] T. Sato, T. Kusakabe, K. Himi, N. Araki, and Y. Konishi, "Ripple-free data-driven dual-rate controller using lifting technique: Application to a physical rotation system," *IEEE Trans. Control Syst. Technol.*, vol. 29, no. 3, pp. 1332–1339, May 2021.
[29] S. Terada, K. Yubai, and J. Hirai, "Correlation-based direct tuning of multivariable controllers with stability constraints based on spectral analysis," in *Proc. IECON 37th Annu. Conf. IEEE Ind. Electron. Soc.*, Nov. 2011, pp. 3352–3357.
[30] K. Yubai, S. Terada, and J. Hirai, "Stability test for multivariable NCbT using input/output data," *IEEJ Trans. Electron., Inf. Syst.*, vol. 131, no. 4, pp. 773–780, 2011.
[31] Q. Jia, "Intersample ripple-free multirate control with applicatio to a hard disk drive servo," *IEEE/ASME Trans. Mechatronics*, vol. 10, no. 3, pp. 314–345, Jul. 2005.
[32] M. Cimino and P. R. Pagilla, "Ripple-free conditions in multirate systems using LTI controllers," in *Proc. Amer. Control Conf.*, Jun. 2010, pp. 1886–1891.
[33] T. Chen and B. Francis, *Optimal Sampled-Data Control Systems*. London, U.K.: Springer, 1995.

TAKAO SATO (Member, IEEE) received the B.Eng., M.Eng., and D.Eng. degrees from Okayama University, in 1997, 1999, and 2002, respectively. He is currently a Professor with the Graduate School of Engineering, University of Hyogo. His research interests include PID control, mechanical systems, and multirate control. He is a member of the Society of Instrumentation and Control Engineers (SICE), Japan, and the Institute of Systems, Control and Information Engineers (ISCIE), Japan.

YUTA SAKAI received the B.Eng. degree from the University of Hyogo, in 2020. He is currently a Student with the Graduate School of Engineering, University of Hyogo.

NATSUKI KAWAGUCHI received the D.Eng. degree from the University of Hyogo, in 2018. He is currently an Assistant Professor with the Graduate School of Engineering, University of Hyogo. His research interests include fault detection and fault tolerant control.

ORLANDO ARRIETA received the B.Sc. and Licentiate degrees in electrical engineering from the University of Costa Rica (UCR), Costa Rica, in 2003 and 2006, respectively, the M.Sc. degree in industrial systems engineering and the Ph.D. degree (Hons.) in PID control field from the Autonomous University of Barcelona (UAB), Barcelona, Spain, in 2007 and 2010, respectively, and the M.B.A. degree from the University of Costa Rica, in 2015. He conducted a postdoctoral research period at the Advanced Controlled Systems Group, UAB. Since 2015, he has been a Full Professor with the Faculty of Engineering, UCR. His main research interests include PID control, process control, and control systems theory and applications. He has been a referee for several international journals and conferences and the coauthor of several contributed books, chapters, and more than 100 refereed international journals/conference papers.